ISSN 1674-1056
http://cpb.iphy.ac.cn
http://iopscience.iop.org/cpb
中国物理 B
Chinese Physics
中国物理
Chinese Physics B

Closed-form internal impedance model and characterization of mixed carbon nanotube bundles for three-dimensional integrated circuits

Qijun Lu(卢启军), Zhangming Zhu(朱樟明), Yintang Yang(杨银堂), Ruixue Ding(丁瑞雪), Yuejin Li(李跃进)
Citation: Chin. Phys. B . 2018, 27(1): 017303. **doi:** 10.1088/1674-1056/27/1/017303

Journal homepage: http://cpb.iphy.ac.cn; http://iopscience.iop.org/cpb

What follows is a list of articles you may be interested in

Dynamic localization of two electrons in AC-driven triple quantum dots and quantum dot shuttles

Jin-Xian Qu(屈晋先), Su-Qing Duan(段素青), Ning Yang(杨宁)
Chin. Phys. B . 2017, 26(12): 127308. **doi:** 10.1088/1674-1056/26/12/127308

Photon-assisted electronic and spin transport through two T-shaped three-quantum-dot molecules embedded in an Aharonov-Bohm interferometer

Jiyuan Bai(白继元), Li Li(李立), Zelong He(贺泽龙), Shujiang Ye(叶树江), Shujun Zhao(赵树军), Suihu Dang(党随虎), Weimin Sun(孙伟民)
Chin. Phys. B . 2017, 26(11): 117302. **doi:** 10.1088/1674-1056/26/11/117302

Polaron effects in cylindrical GaAs/$Al_xGa_{1-x}As$ core-shell nanowires

Hui Sun(孙慧), Bing-Can Liu(刘炳灿), Qiang Tian(田强)
Chin. Phys. B . 2017, 26(9): 097302. **doi:** 10.1088/1674-1056/26/9/097302

Electronic transport properties of single-wall boron nanotubes

Xinyue Dai(代新月), Yi Zhou(周毅), Jie Li(李洁), Lishu Zhang(张力舒), Zhenyang Zhao(赵珍阳), Hui Li(李辉)
Chin. Phys. B . 2017, 26(8): 087310. **doi:** 10.1088/1674-1056/26/8/087310

Toward high-performance two-dimensional black phosphorus electronic and optoelectronic devices

Xuefei Li(李学飞), Xiong Xiong(熊雄), Yanqing Wu(吴燕庆)
Chin. Phys. B . 2017, 26(3): 037307. **doi:** 10.1088/1674-1056/26/3/037307

Closed-form internal impedance model and characterization of mixed carbon nanotube bundles for three-dimensional integrated circuits*

Qijun Lu(卢启军)†, Zhangming Zhu(朱樟明), Yintang Yang(杨银堂), Ruixue Ding(丁瑞雪), and Yuejin Li(李跃进)

School of Microelectronics, Xidian University, Xi'an 710071, *China*

(Received 6 August 2017; revised manuscript received 3 October 2017; published online 17 November 2017)

Based on the complex effective conductivity method, a closed-form expression for the internal impedance of mixed carbon nanotube (CNT) bundles, in which the number of CNTs for a given diameter follows a Gaussian distribution, is proposed in this paper. It can appropriately capture the skin effect as well as the temperature effect of mixed CNT bundles. The results of the closed-form expression and the numerical calculation are compared with various mean diameters, standard deviations, and temperatures. It is shown that the proposed model has very high accuracy in the whole frequency range considered, with maximum errors of 1% and 2.3% for the resistance and the internal inductance, respectively. Moreover, by using the proposed model, the high-frequency electrical characteristics of mixed CNT bundles are deeply analyzed to provide helpful design guidelines for their application in future high-performance three-dimensional integrated circuits.

Keywords: mixed carbon nanotube (CNT) bundle, internal impedance, closed-form expression, complex effective conductivity method

PACS: 73.63.–b, 81.07.De, 85.35.Kt **DOI:** 10.1088/1674-1056/27/1/017303

1. Introduction

Due to their extremely desirable properties of high mechanical and thermal stability, high thermal and electrical conductivity, and large current carrying capacity, carbon nanotubes (CNTs) have been identified as a promising candidate for next generation high-speed interconnect systems.[1–3] According to the number of rolled up graphene sheets, CNTs are classified as single-walled CNTs (SWCNTs, with only one shell) and multi-walled CNTs (MWCNTs, with several concentric shells).[4–6] SWCNTs can be either metallic or semiconducting depending on their chirality, and MWCNTs always behave as metallic conductors.[7] The high intrinsic ballistic resistance associated with an isolated CNT suggests the use of bundles consisting of numerous parallel connected CNTs to realize low-impedance interconnects.[8] It has been proven that CNT interconnects can provide significant performance enhancement with respect to Cu interconnects.[9]

Three-dimensional integrated circuits (3-D ICs) can dramatically enhance chip performance, functionality, and device packing density by stacking multiple layers of active devices vertically.[10,11] Through-silicon vias (TSVs) are essentially cylindrical conducting vias coated with a layer of insulating material residing in silicon substrates for vertical interconnects in 3-D ICs.[12] Recently, TSV arrays filled with CNT bundles were fabricated successfully for 3-D ICs using various methods.[13–16] Meanwhile, the equivalent-circuit models for pure CNT bundles based signal-ground TSV pairs were also proposed.[17–19] However, almost all experiment results show that a realistic CNT bundle is a mixed bundle consisting of SWCNTs and MWCNTs.[20–24] Considering the limitations and cost of the current diameter-controlling methods, adopting pure SWCNT bundles for large-scale integration appears to be impractical in the short term.[25,26] In addition, mixed CNT bundles have the advantages of easy fabrication and the potential benefit of improving the density of the conduction channels. Therefore, they will become the most potential material for high-performance TSVs in future 3-D ICs.

There are few research efforts that have been made to address the modeling and characterization of mixed CNT bundles due to their complexity in structure. The conductance and inductance models for mixed CNT bundles were firstly proposed in Refs. [26] and [27], respectively. However, since the effects of the coupling, frequency, and temperature were not considered, the proposed models are applied only to the conditions of DC and low-frequencies at room temperature. In addition, the models also need numerical calculations, so they are quite inconvenient to use in practice. Furthermore, a similar model for mixed CNT bundles was also proposed, and the effects of the CNT rearrangement inside the bundle on the capacitive and inductive crosstalk were analyzed deeply.[28] More recently, the equivalent-circuit model for mixed CNT bundle based differential TSVs was reported, but the DC conductance model was still used.[29] Therefore, the obtained results are inaccurate.

The objectives of this paper are to propose a closed-

*Project supported by the National Science and Technology Major Project of China (Grant No. 2015ZX03001004) and the National Natural Science Foundation of China (Grant Nos. 61604113, 61625403, 61334003, 61376039, 61574104, and 61474088).

†Corresponding author. E-mail: luqijun2000@126.com; qjlu@xidian.edu.cn

© 2018 Chinese Physical Society and IOP Publishing Ltd

form internal impedance model of cylindrical mixed CNT bundles, and study their high-frequency electrical characteristics to explore the feasibility in the application of future high-performance 3-D ICs. The organization is as follows. In Section 2, a closed-form expression for the internal impedance of mixed CNT bundles is proposed based on the complex effective conductivity method, which serves as the basis of their performance analysis. In Section 3, the proposed model is comprehensively verified against the results of the numerical calculation with various parameters up to 100 GHz. Moreover, a deep analysis of the electrical characteristics of mixed CNT bundles is carried out using the proposed model in Section 4. Finally, some conclusions are drawn in Section 5.

2. Closed-form expression for the internal impedance of mixed CNT bundles

Since an SWCNT, which consists of one shell, is a special case of the MWCNT, mixed CNT bundles can be treated as a combination of multiple MWCNTs.[29] The cross-sectional view of a mixed CNT bundle is shown in Fig. 1, where r is the radius, $D_{\rm in}$ and $D_{\rm out}$ are the inner- and outer-most shell diameters of the MWCNTs, and $\delta = 0.34$ nm is the thickness of each shell, which is equal to the gap between neighboring shells. According to the experimental results in Ref. [22] and modeling in Ref. [5], the ratio of $D_{\rm in}/D_{\rm out}$ can be assumed to be 0.5 approximately.

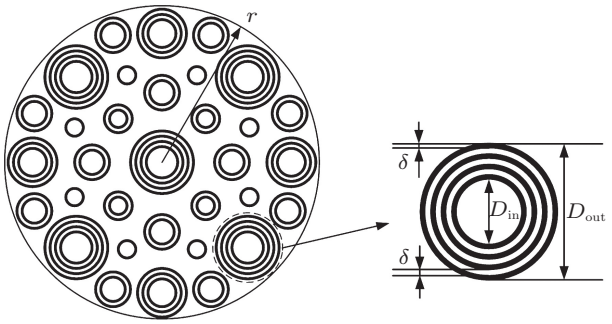


Fig. 1. Cross-sectional view of a mixed CNT bundle.

For MWCNTs, the number of conduction channels per shell is[30]

$$N_{\rm channel} \approx \begin{cases} 2/3, & D < 3d_T/(2T), \\ mTD + n, & D > 3d_T/(2T), \end{cases} \tag{1}$$

where $m = 2.04 \times 10^{-4}$ nm^{-1}·K^{-1}, $n = 0.425$, T is the temperature in Kelvin, D is the diameter of any shell, and $d_T = 1300$ nm·K. The admittance per conduction channel can be given by

$$Y_{\rm channel} = \frac{G_{\rm Q} D}{PD + L}, \tag{2}$$

where $G_{\rm Q} = 2e^2/h$ is the quantum conductance per channel, and

$$P = 1 + \frac{{\rm j}\omega H}{2v_{\rm F}}, \tag{3}$$

$$L = \left(\frac{T}{T_0} - 2\right)\frac{H}{10^3}. \tag{4}$$

Here, e is the electronic charge, h is the Planck constant, H is the length of the mixed CNT bundles, $v_{\rm F} = 8 \times 10^5$ m/s is the Fermi velocity, and $T_0 = 100$ K. It should be noted that P represents the effect of the kinetic inductance. Since the gap between neighboring shells is considerably smaller than the nanotube diameter, the integral method can be used to calculate the parameters of MWCNTS. Therefore, for $D_{\rm out} < 3d_T/(2T)$, the admittance of an MWCNT can be derived as

$$Y_1 = \frac{G_{\rm Q}}{3\delta P^2}\left[\frac{PD_{\rm out}}{2} - L\ln\left(\frac{2PD_{\rm out} + 2L}{PD_{\rm out} + 2L}\right)\right]; \tag{5}$$

and for $D_{\rm out} > 3d_T/(2T)$, it can be derived as

$$Y_2 = \frac{G_{\rm Q}}{3\delta P^2}\left[\frac{9mTPD_{\rm out}^2}{16} + \frac{3(nP - mTL)}{2P} \times \left(\frac{PD_{\rm out}}{2} - L\ln\left(\frac{2PD_{\rm out} + 2L}{PD_{\rm out} + 2L}\right)\right)\right]. \tag{6}$$

According to the practical manufacturing process of mixed CNT bundles,[24] the number of MWCNTs for a given $D_{\rm out}$ follows a Gaussian distribution with a mean diameter $D_{\rm m}$ and a standard deviation σ as

$$N(D_{\rm out}) = \frac{N_{\rm tot}}{\sigma\sqrt{2\pi}}{\rm e}^{-\frac{1}{2}\left(\frac{D_{\rm out} - D_{\rm m}}{\sigma}\right)^2}, \tag{7}$$

where $N_{\rm tot}$ is the total number of MWCNTs determined by the tube density. So, the total admittances of MWCNTs inside a mixed CNT bundle for the two cases can be expressed respectively as

$$Y_{\rm tot1} = \int_0^{\frac{3d_T}{2T}} Y_1 N(D_{\rm out})\,{\rm d}D_{\rm out}, \tag{8}$$

$$Y_{\rm tot2} = \int_{\frac{3d_T}{2T}}^{\infty} Y_2 N(D_{\rm out})\,{\rm d}D_{\rm out}. \tag{9}$$

From Eqs. (5) and (6), it can be observed that equations (8) and (9) need a numerical integration, which is time-consuming and inconvenient to characterize the mixed CNT bundles. To obtain the closed-form expressions, we use the Taylor theorem (due to $N(D_{\rm m} \pm 3\sigma) \approx 0$ and $D_{\rm out} \ll 1$) to approximate the logarithmic function in Eqs. (5) and (6) as

$$\ln\left(\frac{2PD_{\rm out} + 2L}{PD_{\rm out} + 2L}\right) \approx a(D_{\rm out} - D_{\rm m})^2 + b(D_{\rm out} - D_{\rm m}) + c, \tag{10}$$

where

$$a = \frac{-P^2\left(3L^2 + 2PD_{\rm m}L\right)}{2(PD_{\rm m} + L)^2(PD_{\rm m} + 2L)^2}, \tag{11}$$

$$b = \frac{PL}{(PD_{\rm m} + L)(PD_{\rm m} + 2L)}, \tag{12}$$

$$c = \ln\left(\frac{2PD_{\rm m}+2L}{PD_{\rm m}+2L}\right). \tag{13}$$

In addition,

$$\int_{-\infty}^{x} \mathrm{e}^{\frac{-u^2}{2}}\,\mathrm{d}u \approx \frac{\sqrt{2\pi}}{1+\mathrm{e}^{\alpha x}}, \tag{14}$$

where $\alpha = -1.702$.[31] Therefore, the closed-form expressions for $Y_{\rm tot1}$ and $Y_{\rm tot2}$ can be further derived, respectively, as

$$Y_{\rm tot1} \approx \frac{G_{\rm Q}N_{\rm tot}}{3\delta P^2} \times \left[\frac{1}{\sqrt{2\pi}}A\,\mathrm{e}^{-t^2/2} - B\frac{1}{1+\mathrm{e}^{-\alpha t}}\right], \tag{15}$$

$$\begin{aligned} Y_{\rm tot2} \approx{}& \frac{G_{\rm Q}N_{\rm tot}}{3\delta P^2} \times \left[\frac{1}{\sqrt{2\pi}}\left(\frac{9mTP(\sigma^2 t+2\sigma D_{\rm m})}{16}\right.\right. \\ &\left. - \frac{3(nP-mTL)}{2P}A\right)\mathrm{e}^{-t^2/2} + \frac{\mathrm{e}^{-\alpha t}}{1+\mathrm{e}^{-\alpha t}} \\ &\left.\times\left(\frac{9mTP(\sigma^2+D_{\rm m}^2)}{16} - \frac{3(nP-mTL)}{2P}B\right)\right], \end{aligned} \tag{16}$$

where

$$A = La\sigma^2 t + Lb\sigma - \frac{1}{2}P\sigma, \tag{17}$$

$$B = La\sigma^2 + Lc - \frac{1}{2}PD_{\rm m}, \tag{18}$$

$$t = \left(\frac{2d_T}{3T} - D_{\rm m}\right)/\sigma. \tag{19}$$

Furthermore, the complex effective conductivity of the mixed CNT bundles can be obtained by

$$\sigma_{\rm eff} = \frac{(Y_{\rm tot1}+Y_{\rm tot2})H}{\pi r^2}. \tag{20}$$

The accurate expression for the internal impedance of cylindrical conductors is[32]

$$Z = \frac{KH}{2\pi r\sigma_{\rm eff}} \cdot \frac{I_0(Kr)}{I_1(Kr)}, \tag{21}$$

where $K = (\omega\mu_0\sigma_{\rm Cu})^{1/2}\,\mathrm{e}^{\mathrm{j}(\pi/4)}$, I_0 and I_1 are the modified Bessel functions of the first kind of order zero and one. To remove the Bessel functions, it is approximated as[33]

$$Z \approx \frac{KH\cdot\coth(0.777Kr)}{2\pi r\sigma_{\rm eff}} + \frac{0.356H}{\pi r^2\sigma_{\rm eff}}. \tag{22}$$

Note that the approximate accuracy mainly depends on the parameter Kr. The maximum error of the resistance is 4% occurring when $|Kr| = 5$ and that of the inductance is 5% occurring when $|Kr| = 3.5$. Substituting Eq. (20) into Eq. (22), we can easily obtain the internal impendence of the mixed CNT bundles. Moreover, their resistance and internal inductance can be given by

$$R = \mathrm{Re}(Z), \tag{23}$$

$$L = \frac{\mathrm{Im}(Z)}{\omega}. \tag{24}$$

3. Verification of the proposed model of mixed CNT bundles

Figures 2 and 3 compare the resistances and the internal inductances of mixed CNT bundles obtained from the closed-form expression and the numerical calculation up to 100 GHz, respectively, with various mean diameters, standard deviations, and temperatures. Here, $r = 5$ μm, $H = 100$ μm, and $N_{\rm tot} = 7.854\times10^4$ (the tube density is assumed as 10^3 μm^{-2}). It should be noted that the results of the numerical calculation are obtained using Eqs. (5)–(9), (20), and (21) with the Simpson numerical integral, and those of the closed-form expression using Eqs. (5), (6), (15), (16), (20), and (22). It can be observed that the results of the closed-form expression agree extremely well with those of the numerical calculation in the whole frequency range considered, with maximum errors of 1% and 2.3% for the resistance and the internal inductance, respectively. The accuracy of the proposed model can be further improved by using higher-order polynomials to approximate the logarithmic function in Eq. (10). In addition, the resistance increases, and the internal inductance decreases, respectively, at high frequencies due to the skin effect. However, similar

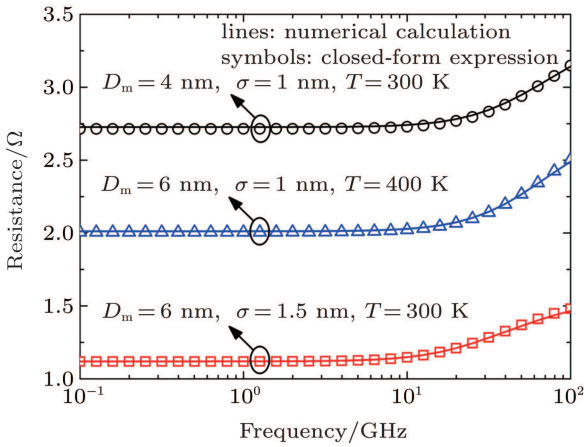


Fig. 2. (color online) Comparison of the resistances of mixed CNT bundles obtained from the closed-form expression and the numerical calculation.

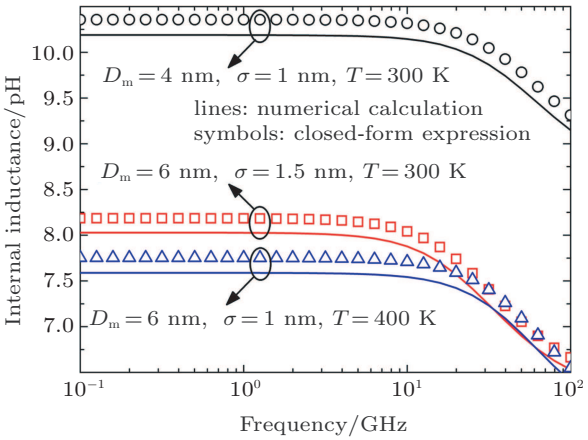


Fig. 3. (color online) Comparison of the internal inductances of mixed CNT bundles obtained from the closed-form expression and the numerical calculation.

to pure MWCNT bundles, the corresponding rates of mixed CNT bundles are obviously smaller than those of Cu interconnects. So they are very suitable for next generation high-speed interconnect systems.

4. Analysis of electrical characteristics of mixed CNT bundles

For mixed CNT bundles in the actual application, the number of CNTs is large enough so that the effect of the quantum capacitance can be neglected. In addition, their electrostatic capacitance and external inductance are the same as those of Cu interconnects, respectively. Therefore, the primary distinction between mixed CNT bundles and Cu interconnects is the internal impedance including the resistance and internal inductance. In this section, we will mainly analyze the effects of the mean diameter $D_{\rm m}$, standard deviation σ, and temperature T on the resistance and internal inductance of mixed CNT bundles. The reference values are chosen as $D_{\rm m} = 6$ nm, $\sigma = 1$ nm, and $T = 300$ K, and all other parameters are the same as those in Fig. 2.

4.1. Resistance

As the mean diameter $D_{\rm m}$ increases, the total number of conduction channels increases so that the resistance rapidly decreases, as shown in Fig. 4. However, the rate decreases gradually and is almost frequency-independent. Furthermore, it can be observed that the resistance increases at high frequencies due to the skin effect, and the rate increases as the mean diameter $D_{\rm m}$ increases. When the frequency increases from 1 GHz to 100 GHz, the resistance increases by about 16% and 47% with the mean diameter $D_{\rm m}$ of 4 nm and 8 nm, respectively. Therefore, the smaller the mean diameter $D_{\rm m}$ is, the weaker the influence of the skin effect. However, similar to pure CNT bundles, the rate of increase of the resistance decreases rapidly at very high frequencies due to the existence of large kinetic inductance or large momentum relaxation time. It is obvious that the resistance of mixed CNT bundles with larger mean diameter $D_{\rm m}$ starts saturating at a relatively lower frequency and vice versa.

Although the standard deviation σ is a dominant factor determining the distribution of the diameter of MWCNTs inside a mixed CNT bundle, its effect on the total number of conduction channels is quite small. Therefore, the resistance decreases slowly as the standard deviation σ increases, as shown in Fig. 5. When the standard deviation σ increases from 0.5 nm to 1.5 nm, the resistance increases by about 11.2% and 7.1% with the frequency of 1 GHz and 100 GHz, respectively. It is shown that the effect of the standard deviation σ on the resistance weakens as the frequency increases. On the other hand, the rate of increase of the resistance due to the skin effect increases slowly as the standard deviation σ increases. In other words, the influence of the skin effect is slightly enhanced.

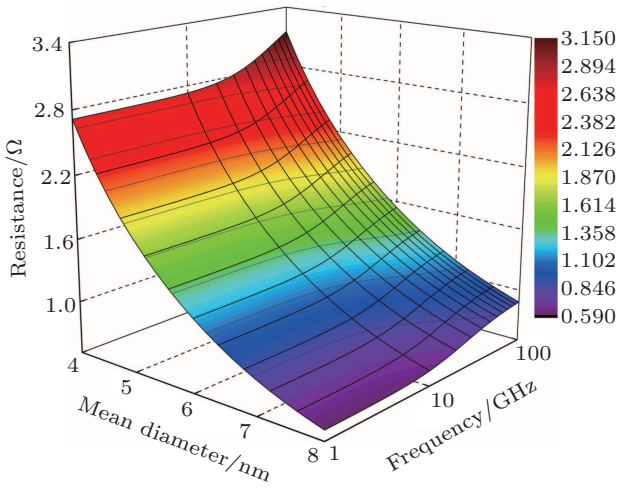


Fig. 4. (color online) Resistance of mixed CNT bundles obtained from the proposed model versus the mean diameter and frequency.

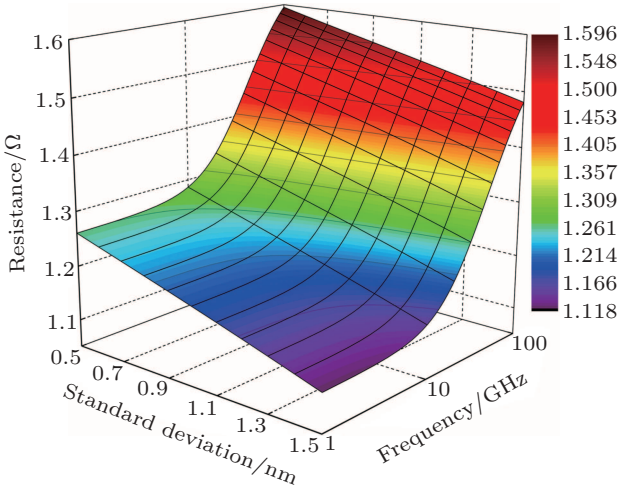


Fig. 5. (color online) Resistance of mixed CNT bundles obtained from the proposed model versus the standard deviation and frequency.

As the temperature T increases, although the number of conduction channels of larger diameter MWCNTs increases linearly, which can effectively decrease the resistance, the resistance still increases sharply and the increasing-speed is almost frequency-independent, as shown in Fig. 6. This is due to the fact that the mean free path quadratic decreases as the temperature T increases, so that the resistance of all conduction channels increases rapidly.[34,35] Furthermore, it can be observed that the rate of increase of the resistance due to the skin effect decreases as the temperature T increases. When the frequency increases from 1 GHz to 100 GHz, the resistance increases by about 29.1% and 24.8% with the temperature T of 300 K and 400 K, respectively. Therefore, the higher the temperature T is, the weaker the influence of the skin effect, but this effect is quite small since the gap between these two proportions is not obvious. This property is similar to that of Cu

interconnects. Accordingly, the resistance of mixed CNT bundles with higher temperature T starts saturating at a relatively higher frequency and vice versa.

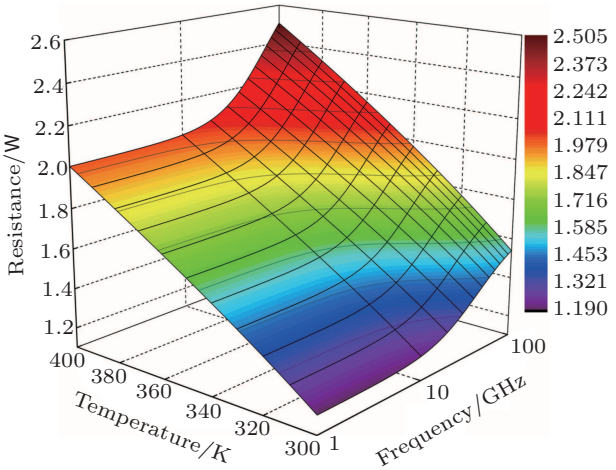


Fig. 6. (color online) Resistance of mixed CNT bundles obtained from the proposed model versus the temperature and frequency.

4.2. Internal inductance

Similar to the case of the resistance, as the mean diameter D_m increases, the internal inductance decreases rapidly due to the increase of the number of conduction channels, and the decreasing-speed also decreases gradually, as shown in Fig. 7. Since the magnetic inductance tends to be zero at high frequencies, and the kinetic inductance is becoming a dominant factor determining the total internal inductance, which decreases rapidly as the number of conduction channels increases. Therefore, the rate increases as the frequency increases. Furthermore, it can be observed that the rate of decrease with the frequency of the internal inductance increases as the mean diameter D_m increases. When the frequency increases from 1 GHz to 100 GHz, the internal inductance reduces by about 9.6% and 25% with the mean diameter D_m of 4 nm and 8 nm, respectively. Actually, this property of the internal inductance is also produced by the skin effect. Similar to the case of the resistance, the internal inductance of mixed CNT bundles with larger mean diameter D_m also starts saturating at a relatively lower frequency and vice versa.

It is obvious that the internal inductance decreases slowly as the standard deviation σ increases, as shown in Fig. 8. When the standard deviation σ increases from 0.5 nm to 1.5 nm, the internal inductance reduces by about 0.7% and 2.6% with the frequency of 1 GHz and 100 GHz, respectively. It is shown that the effect of the standard deviation σ on the internal inductance enhances as the frequency increases, contrary to the case of the resistance. It can also be observed that the rate of increase of the internal inductance due to the skin effect is almost the same as the standard deviation σ increases since its influence on the skin effect is quite small.

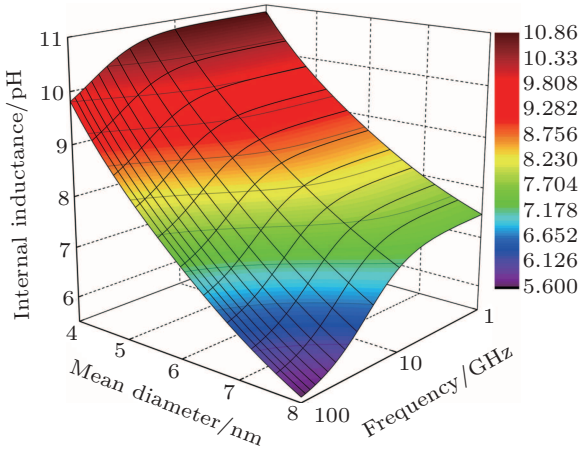


Fig. 7. (color online) Internal inductance of mixed CNT bundles obtained from the proposed model versus the mean diameter and frequency.

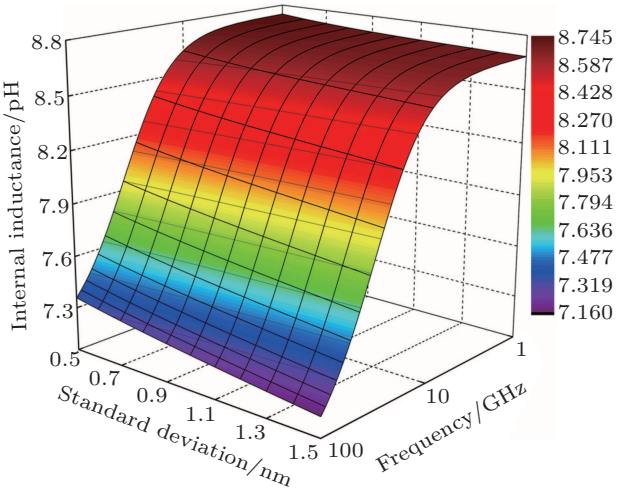


Fig. 8. (color online) Internal inductance of mixed CNT bundles obtained from the proposed model versus the standard deviation and frequency.

The internal inductance decreases as the temperature T increases and the rate is almost frequency-independent due to the linear increase of the number of conduction channels of larger diameter MWCNTs inside a mixed CNT bundle, as shown in Fig. 9. Moreover, it can be observed that the rate

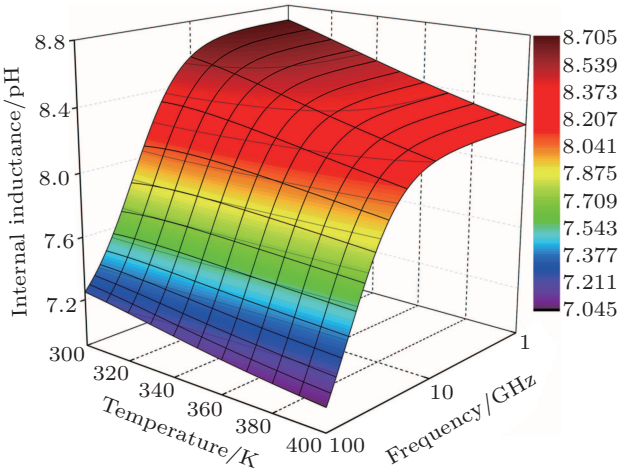


Fig. 9. (color online) Internal inductance of mixed CNT bundles obtained from the proposed model versus the temperature and frequency.

of increase of the internal inductance due to the skin effect decreases slowly as the temperature T increases. When the frequency increases from 1 GHz to 100 GHz, the internal inductance reduces by about 16.7% and 14.6% with the temperature T of 300 K and 400 K, respectively. This further indicates that the influence of the skin effect is almost temperature-independent. In addition, the saturation property of the internal inductance of mixed CNT bundles at very high frequencies when the temperature T varies is similar to that of their resistance.

5. Conclusion

A closed-form expression for the internal impedance of mixed CNT bundles is proposed in this paper. The results of the proposed model agree extremely well with those of the numerical calculation up to 100 GHz, with maximum errors of 1% and 2.3% for the resistance and the internal inductance, respectively. In order to provide helpful design guidelines for mixed CNT bundles in future 3-D ICs, the effects of the mean diameter, standard deviation, and temperature on their internal impedance are analyzed deeply using the proposed model. It is shown that both the resistance and the internal inductance decrease rapidly as the mean diameter increases. Meanwhile, the two corresponding rates remain almost the same and increase as the frequency increases. However, they are decreasing slowly as the standard deviation increases since its effect on the total number of conduction channels is quite small. In addition, the resistance increases rapidly and the internal inductance decreases, respectively, as the temperature increases, and the corresponding rates are both almost frequency-independent.

References

[1] Hosiny N H and Badawi 2015 *Chin. Phys. B* **24** 105101
[2] Zhang Q, Li K W, Fan Q X, Xia X G, Zhang N, Xiao Z J, Zhou W B, Yang F, Wang Y C, Liu H P and Zhou W Y 2017 *Chin. Phys. B* **26** 028802
[3] Bafandeh N, Larijani M M, Shafiekhani, Hantehzadeh M R and Sheikh N 2016 *Chin. Phys. Lett.* **33** 117801
[4] Yang J Q, Li X J, Liu C M, Ma G L and Gao F 2015 *Chin. Phys. B* **24** 116103
[5] Li H, Yin W Y, Banerjee K and Mao J F 2008 *IEEE Trans. Electron Devices* **55** 1328
[6] Ahmad Z, Karimov K S and Touati F 2016 *Chin. Phys. B* **25** 028801
[7] Giustiniani A, Tucci V and Zamboni W 2010 *IEEE Trans. Electron Devices* **57** 1978
[8] Sarto M S, Tamburrano A and Amore M D 2009 *IEEE Trans. Nanotechnol.* **8** 214
[9] Li H and Banerjee K 2009 *IEEE Trans. Electron Devices* **56** 2202
[10] Qian L B, Zhu Z M, Xia Y S, Ding R X and Yang Y T 2014 *Chin. Phys. B* **23** 038402
[11] Liu X X, Zhu Z M, Yang Y T, Ding R X and Li Y J 2016 *Chin. Phys. B* **25** 118401
[12] Liu E X, Li E P, Ewe W B, Lee H M, Lim T G and Gao S 2011 *IEEE Trans. Microw. Theory Techn.* **59** 1454
[13] Vollebregt S, Banerjee S, Tichelaar F D and Ishihara R 2015 *Proceedings of the IEEE International Interconnect Technology Conference and IEEE Materials for Advanced Metallization Conference*, May 18–21, 2015, Grenoble, France, p. 281
[14] Sofela S O, Younes H, Jelbuldina M, Saadat I and Ghaferi A A 2015 *Proceedings of the IEEE International Interconnect Technology Conference and IEEE Materials for Advanced Metallization Conference*, May 18–21, 2015, Grenoble, France, p. 289
[15] Ghosh K, Yap C C, Tay B K and Tan C S 2013 *Proceedings of the IEEE International 3D Systems Integration Conference*, October 2–4, 2013, San Francisco, CA, USA, p. 1
[16] Wang T, Chen S, Jiang D, Fu Y, Jeppson K, Ye L and Liu J 2012 *IEEE Electron Device Lett.* **33** 420
[17] Zhao W S, Yin W Y and Guo Y X 2012 *IEEE Trans. Electromagn. Compat.* **54** 149
[18] Liu Y F, Zhao W S, Yong Z, Fang Y and Yin W Y 2014 *IEEE Trans. Nanotechnol.* **13** 488
[19] Xu C, Li H, Suaya R and Banerjee K 2010 *IEEE Trans. Electron Devices* **57** 3405
[20] Zhu L B, Xu J W, Xiu Y H, Sun Y Y, Hess D W and Wong C P 2006 *Carbon* **44** 253
[21] McEuen P L, Fuhrer M S and Park H 2002 *IEEE Trans. Nanotechnol.* **1** 78
[22] Li H J, Lu W G, Li J J, Bai X D and Gu C Z 2005 *Phys. Rev. Lett.* **95** 086601
[23] Li J, Ye Q, Casssell A, Ng H T, Stevens R, Han J and Meyyappan M 2003 *Appl. Phys. Lett.* **82** 2491
[24] Sato S, Nihei M, Mimura A, Kawabata A, Kondo D, Shioya H, Iwai T, Mishima M, Ohfuti M and Awano Y 2006 *Proceedings of the IEEE International Interconnect Technology Conference*, June 5–7, 2006, Burlingame, CA, USA, p. 230
[25] Cheung C L, Kurtz A, Park H and Lieber C M 2002 *J. Phys. Chem.* **106** 2429
[26] Haruehanroengra S and Wang W 2007 *IEEE Electron Device Lett.* **28** 756
[27] Wang W, Haruehanroengra S, Shang L and Liu M 2007 *IET Micro Nano Lett.* **2** 35
[28] Subash S, Kolar J and Chowdhury M H 2013 *IEEE Trans. Nanotechnol.* **12** 3
[29] Qian L B, Xia Y S and Shi G 2016 *IEEE Trans. Nanotechnol.* **15** 155
[30] Naeemi A and Meindl J D 2006 *IEEE Electron Device Lett.* **27** 338
[31] Bowling S R, Khasawneh M T, Kaewkuekool S and Cho B R 2009 *J. Ind. Eng. Manage.* **2** 114
[32] Schelkunoff S A 1934 *Bell Syst. Tech. J.* **13** 532
[33] Wedepohl L M and Wilcox D J 1973 *Proc. Inst. Elect. Eng.* **120** 253
[34] Chiariello A G, Maffucci A and Miano G 2013 *IEEE Trans. Comp., Packag. Manuf. Technol.* **3** 1926
[35] Qian L B, Xia Y S, Shi G, Wang J, Die Y Y and Du S M 2017 *IEEE Trans. Nanotechnol.* **16** 901